NASA Technical Memorandum 100797

CFD Validation Experiments for Internal Flows

Louis A. Povinelli
Lewis Research Center
Cleveland, Ohio

Prepared for the
Symposium on Validation of Computational Fluid Dynamics
sponsored by the AGARD Fluid Dynamics Panel
Lisbon, Portugal, May 2–5, 1988

NASA

CFD VALIDATION EXPERIMENTS FOR INTERNAL FLOWS

Louis A. Povinelli
National Aeronautics and Space Administration
Lewis Research Center
Cleveland, Ohio 44135 U.S.A.

SUMMARY

CFD validation experiments at NASA Lewis Research Center are described in this paper. The material presented summarizes the research in three areas: Inlets, Ducts and Nozzles; Turbomachinery; and Chemically Reacting Flows. The specific validation activities are concerned with shock-boundary layer interactions, vortex generator effects, large low speed centrifugal compressor measurements, transonic fan shock structure, rotor/stator kinetic energy distributions, stator wake shedding characteristics, boundary layer transition, multiphase flow and reacting shear layers. These experiments are intended to provide CFD validation data for the internal flow fields within aerospace propulsion system components.

E-3973

INTRODUCTION

Internal fluid mechanics research at NASA Lewis is directed toward an improved understanding of the flow phenomena affecting aerospace propulsion systems, and the application of this knowledge in the formulation of accurate predictive codes. In order to achieve this objective, research is conducted which involves both detailed experimentation and analysis. A close coupling between the experimental and the code development work is a critical feature of this research. The insights gained from the experimental work are represented by mathematical models that form the basis for code development. The resulting codes are then tested by comparing them with appropriate experiments in order to ensure their validity and determine their applicable range. Subsequent improvements and refinements lead to validated numerical codes.

The definition of CFD code validation as used in this paper, is that adopted by the NASA Aeronautics Advisory Committee (Ref. 1); wherein a key item is the ability of a numerical code to accurately model the critical physics of the flow. In addition, validation may only occur when the accuracy and limitations of both the experimental data and the code's algorithm are known and understood over a range of specified parameters.

This paper is concerned with a number of experiments which are underway in order to provide validation information for internal flow codes, as well as to provide improved understanding of the flow physics. Previous publications by this author have addressed the assessment and validation for turbomachinery, inlet and ducting flows (Refs. 2 to 5). In this paper, those areas are addressed further along with chemically reacting flows. For each of the three subject areas, material will be presented on the experimental validation programs as well as the computational codes used.

INLETS, DUCTS AND NOZZLES FLOWS

The inlet, duct, and nozzle research is illustrated in Table I and includes experimental work in transition ducts, offset ducts, diffusers with vortex generators, inlet shock-boundary layer interactions, diffuser and nozzle jet mixing, inlet and diffuser boundary layer bleed and inlet/nozzle separation flow physics. The critical physics to be modeled (Table I) for these experiments are the phenomena associated with turbulence, boundary layer separation, vortex generation, bleed, transition, heat transfer and real gases effects. All of the research activity described above may be described according to three major classifications of flow phenomena: highly three-dimensional flow fields, shock boundary layer interactions and shear layer control. The importance of these three flow phenomena result from aircraft/propulsion requirements such as engine locations, thrust vectoring, maneuverability, high-Mach number flight, and shorter/lighter components. Specific elements of the research program are shown in Fig. 1 for each of the three flow field phenomena. Only two of the elements, however, will be presented here. The first is the shock boundary layer interaction phenomena which will be illustrated with a description of the normal shock research activity. The second, shear layer control, will be illustrated with vortex generator research. Additional information on these activities are described in Ref. 6.

Normal shock-boundary layer interaction. Figure 2 illustrates the nature of the normal shock interaction for two Mach numbers, 1.3 and 1.6. Schlieren photographs and oil streak photographs are shown for both Mach numbers. These data were obtained in the NASA Lewis 1-by-1-foot supersonic wind tunnel (Ref. 7). The Schlieren photographs show a view of the shock interaction, while the oil streaks illustrate the flow field details along the side wall. At both Mach numbers, the Schlieren photographs show the shock has a lamda structure near the boundary layer. The sidewall oil streaks reveal a major difference in the flow field for the two Mach numbers. At Mach 1.3 the flow remains uniform and passes through the shock with no major alteration. At Mach 1.6,

the adverse pressure gradient across the shock is strong enough to force the boundary layer to separate from the tunnel walls and to form the closed separation bubble shown in Fig. 2. Both the Mach 1.3 and 1.6 flow fields were surveyed in detail using nonintrusive laser anemometry. Results are shown in Fig. 3 for the Mach 1.6 case in two planes within the flow field. The top set of Mach contours illustrates the nature of the flow field in a cross plane downstream of the shock. The lower set of Mach contours shows the development of the flow field within a vertical plane passing through the centerline of the test section. The separated region in the vicinity of the initial interaction causes the actual flow area to contract downstream of the initial shock, leading to a reacceleration of the flow to supersonic Mach numbers. The flow then shocks down again, reaccelerates again due to the thickened boundary layer, and finally shocks down a final time. The lower portion of Fig. 3 is repeated as the lower portion of Fig. 4, namely the Mach contours measured with LV in a vertical plane passing through the centerline of the test section at Mach 1.6. The upper portion of Fig. 4 is a two-dimensional Navier-Stokes computation of the same flow field. Although the computation captures the initial features fairly well in the vicinity of the first shock, in the downstream region, none of the flow features is adequately replicated. This result is to be expected since the experimental data have shown the strong three-dimensionality of the flow. This comparison points out the need for three-dimensional computational methods for computing such flow fields. However, in the case of the Mach 1.3 flow, excellent agreement was obtained between experiments and computations. Again, this result is consistent with the experimentally observed two-dimensionality of the flow field. Additional insight and understanding of the experimental data were obtained through the use of computer graphics. The experimental data sets were modified to a format that was originally developed for presenting computational results. The three-dimensional data contours were then displayed and set into motion on the screen. A perspective may be gained much more quickly from these rotating images than can be obtained by looking at a series of two-dimensional or even three-dimensional plots.

Vortex generators in diffusing offset duct. Figure 5 illustrates a research model and facility that was used in an experiment to assess the performance of vortex generators in a 30° to -30° diffusing S duct (Ref. 8). The duct had a length-to-diameter ratio of 5.0, an offset-to-diameter ratio of 1.34, and an exit-to-inlet area of 1.51. Initial experiments with the duct identified the location of a separated flow region as shown by the surface oil streak photograph. Three pairs of vortex generators were then added to the duct surface just upstream of the separated region to control the separation. They were set at incidence angles of ±16° to form three pairs of counter rotating vortices. The azimuthal locations were at -38°, 0°, +38° as measured from the inside of the bend. The flow was turbulent with a Mach number of 0.6 and a Reynolds number (based on diameter) of 1.76×10^6. The initial boundary layer thickness was 0.1 times the initial duct radius. A comparison of total pressure contours at various locations down the length of the duct with the vortex generators in place is shown in Fig. 6. The experimental data were obtained by surveying the flow field with a total pressure probe. The computational results are from a three-dimensional parabolized Navier-Stokes code. The computations involve a method for modeling the streamwise vorticity due to the presence of the vortex generators and the decay of the vorticity. The computed total pressure contours are shown in the lower portion of Fig. 6, and the experimental data are shown in the upper portion. The comparisons show good agreement in all of the qualitative features, including the discrete effect of the three sets of vortex generators. Comparison of experimental and computational data for the duct without generators also showed good global agreement. In order to handle the region of separated flow in the absence of vortex generators, a flare approximation was used in the PNS code to march downstream of the separation bubble.

TURBOMACHINERY FLOWS

The second subject area is concerned with turbomachinery validation. Table II illustrates the program elements underway and includes Euler, Average-Passage, and Reynolds averaged steady and unsteady Navier-Stokes codes. The critical physics to be modeled include turbulence, boundary-layer transition, end wall and blade surface boundary layer interactions. Use of the unsteady Navier-Stokes approach reflects the fact that turbomachinery flow is fundamentally unsteady or time dependent, and may be further complicated by random disturbances.

Turbomachinery research at NASA Lewis currently involves a variety of computational and experimental approaches as shown in Fig. 7. On the far left of the computational approaches, the time accurate Navier-Stokes equations are capable of resolving all relevant time scales in turbomachinery flow. However, enormous computer power is required. In order to readily obtain solutions, a variety of averages are made, which result in a loss of information or resolution in the equations. It also introduces more unknowns and requires additional empirical data. As one moves to the left of the experimental path, increasing detail in the time domain is obtained, whereas moving to the right increases the averaging of temporal behavior. Current research at NASA Lewis focuses on the analytic range from the Reynolds averaged Navier-Stokes equations to the average passage equations. The experimental emphasis is on high response time resolved measurements and on laser anemometry measurements. Further information regarding these activities may be found in Ref. 9.

Large low speed centrifugal compressor. Centrifugal compressors feature large surface area and small exit-passage heights. Viscous flow effects, therefore, have a

major impact on the flowfield within these compressors. The inability to accurately predict and measure these flows contributes in large part to the inherently lower efficiency of centrifugal compressors relative to axial flow compressors. The large low-speed centrifugal compressor shown in the background of Fig. 8 has been designed specifically to provide flow modeling and viscous code validation data for centrifugal compressors. The impeller was designed to be aerodynamically similar to high performance, high speed centrifugal compressors such as the small 6:1 pressure ratio impeller shown in the photograph. The low speed impeller has a tip diameter of 50 in. and a rotational speed of 1950 rpm. Inlet and exit blade heights are 9 and 4.75 in., respectively. The large size and low speed of the new impeller generate viscous flow regions (such as blade and endwall boundary layers) and tip clearance flows which are large enough to measure in detail with laser anemometry. Figure 9 shows an overall view of the facility and 10 shows the rotor. Figure 11 shows the location and type of instrumentation currently being installed. It is anticipated that experimental data will be obtained during this year. Future plans include replacing the centrifugal rotor with a four stage axial compressor. A quasi-three-dimensional Navier-Stokes turbomachinery code has been developed and applied for the large low speed centrifugal analysis (Ref. 10). The code includes the effects of radius change, stream surface thickness and rotation. The unsteady Navier-Stokes equations are solved in finite difference form using an explicit Runge-Kutta algorithm with a spatially varying time step and multigrid convergence acceleration. The flow in the 6:1 pressure ratio centrifugal impeller has been calculated on a 161x33 grid. Relative Mach number contours in Fig. 12 show a supersonic bubble on the leading edge terminated by a shock. Rotational effects make the suction surface boundary layer thin, the pressure surface boundary layer thick, and they cause the wake to leave the trailing edge in a spiral. The calculations require about $3x10^6$ words of storage and 1.5 min of CPU time on a Cray X-MP. The flow in the new, large low-speed rig has also been calculated and is shown on the right. The ability to validate this and other codes in the large low-speed rig will generate confidence in the high speed calculations where validation may not be possible.

Transonic fan shock structure. A second example of the turbomachinery research is concerned with the shock behavior in a transonic fan. Current axial fan and compressor design systems do not account for the three-dimensionality of passage shocks. Figure 13 is an example of a high speed experiment to determine shock structure physics (Ref. 11). Shock locations determined from laser anemometry measurements are shown on blade-to-blade surfaces of revolution in the upper portion of the figure. Three different views of the same data, as displayed on a graphics workstation, are shown in the bottom portion of the figure. A significant spanwise lean of the shock surface is evident in these three-dimensional views.

Comparisons of the measured shock strength and location with an Euler code (Denton) are shown in Fig. 14 for two operating conditions; peak efficiency and near stall. The comparisons show that the spanwise location of the computed and measured sonic lines are in reasonable agreement over the range of operating conditions. A comparison of the measured and the idea shock strengths is shown in Figs. 14(b) and (c).

Compressor turbulent kinetic energy distribution. Measurements of the unsteady flowfield within a compressor stator operating downstream of a transonic fan rotor have been obtained using laser anemometry. Figure 15 shows a contour plot of the ensemble-averaged unresolved unsteadiness in the stator (includes unsteadiness due to both turbulence and vortex shedding) for one rotor/stator relative position. Areas of unresolved unsteadiness contain fluid which is in the rotor-blade wake. As the rotor blades rotate past the stator blades, the rotor wakes are convected through the stator row by the absolute flow velocity and, subsequently, chopped by the stator blades. Data obtained at additional times during the blade passing cycle have been used to produce a movie sequence which illustrates the ensemble-averaged wake dynamics and its effect on the stator flowfield. These data will be used in order to obtain closure modeling terms needed for turbomachinery codes.

Fan rotor vortex shedding. Karman vortex streets are known to exist in blunt body wakes over a wide flow regime. However, the existence of vortex streets in transonic fan and compressor blade wakes was not generally anticipated since these blades have thin trailing edges. Laser anemometry measurements obtained in the wake of a transonic fan blade indicated two distinct states of flow in the central portion of the wake (Ref. 12). This behavior is consistent with that which would be displayed by a Karman vortex street, see Fig. 16. A simple vortex street model was constructed in an attempt to explain the experimental measurements. The model qualitatively agreed with the bimodal character of the velocity measurements. The model was used to explain the highly unsteady nature of high response pressure measurements made in the same wake flowfield. This research typifies the manner in which advanced measurements coupled with modeling improve our understanding of complex flow phenomena.

Boundary layer transition. Boundary layer transition is a critical feature that needs to be modeled for each of the three general areas discussed in this paper. Transition plays an especially vital role in the gas-side heat transfer within turbomachinery as well as in high speed components. A fundamental experimental activity is underway which is investigating the nature of the transition mechanism. In particular, the differences in the classical boundary layer transition process and the bypass transition are being studied subject to variations in the external free stream turbulence level. Simultaneous hot wire and hot film measurements were made in a flat plate boundary layer tunnel. The transition location was determined by three methods which used

either the mean velocity profiles, the rms profiles or the intermittency measurements. By-pass transition was found to occur at freestream turbulence levels of 6.5 percent whereas the Tollmien-Schlicting path to transition was observed at 3.5 percent. Even though freestream disturbances varied only by a factor of ~2, the disturbances within the boundary layer vary by two orders of magnitude within the frequency range where linear stability theory would predict amplification.

Figure 17 shows a schematic of the tunnel used for the study as well as a carpet plot of the simultaneous hot film measurements along the flat plate surface. The progression and growth of turbulence along the surface can be readily observed. Continuing research will involve the investigation of wall heating effects.

CHEMICALLY REACTING FLOWS

The third subject area to be presented is that of chemically reacting flows. The relevant numerical codes are the steady and time accurate Reynolds averaged Navier-Stokes and Direct Numerical Simulation, as shown in Table III. In this category of flows, the critical physics to be modeled include turbulence-combustion interactions and chemical kinetics. The experimental activity involves multi-phase flows, phase interactions, planar reacting shear layers, radiation characteristics and shock tube measurements. Due to the complexity of the combustion process in propulsion devices, a stepwise approach is being taken in developing an improved understanding of the processes; see Fig. 18. Following this approach, the fluid mechanics of certain flows are studied in the absence of combustion; combustion chemistry is studied principally from the viewpoint of kinetics; and finally the interaction of the turbulence (fluid mechanics) and the chemistry becomes the focal point. Further information on these activities may be found in Ref. 13.

Multiphase flows. Particle laden jets were studied in order to assess the capability of current two-phase flow models (Ref. 14). An air jet containing solid glass beads (39 μm, Sauter mean diameter) discharged downward into a still environment. Particle laden jets with three swirl numbers were studied. Nonintrusive measurements of velocity were obtained with a two channel laser velocimeter. Particle size and velocity were measured with a phase/doppler particle anemometer. The gas phase was seeded with nominal 1 μm diameter aluminum oxide power to measure gas phase velocities. Figure 19 shows typical results. A contour plot of experimentally measured axial velocity of the gas phase (left side) and particle phase (right side) is illustrated. It is evident that, initially, the gas phase has a higher velocity than the particle phase. The particles are initially accelerated by the gas phase and then their velocity begins to decay. Because of their inertia, the rate of decay of axial velocity is slower for the particles than the gas. Also shown in Fig. 19 are predictions from the stochastic separated flow (SSF) model at 10 diameters downstream of the tube exit. This model tracks particle trajectories in the computed gas phase flowfield and allows momentum exchange between phases. The model also considers effects of gas-phase turbulence on particle trajectories. Predictions from the model show reasonable agreement with the data.

Turbulent reacting flow. A free shear layer experiment is currently underway in order to understand the coupling between fluid dynamics and combustion. The activity will also provide validation data. The experimental apparatus is shown in Fig. 20 and consists of two separate channels which merge into a combustion chamber with a splitter plate. The facility features continuous flow of air in one channel and hydrogen/nitrogen in the other. Mach numbers are limited to less than sonic. Upstream heating of air without contamination and high heat release in the combustion section are additional features of this experiment. Interactions between the combustion process and duct pressure oscillations will be principal foci for study.

Initial computations of the time-evolving shear layer without reaction have been carried out using a time accurate, two-dimensional shear layer code. This code employs a Navier-Stokes finite volume method with a two equation turbulence model. It has second order accuracy in both time and space. Figure 21 shows the computed vorticity contours for a shear layer at a Reynolds number of 1×10^5. Positive and negative vorticity contours originate at the boundary layers, specified at the inlet of the computational domain. Forcing is applied at a long wavelength, and smaller scale vorticities spontaneously develop as a result of the natural instability of the layer. These small scale vorticities cluster on the scale of the longer, forced wavelength. Small pockets of positive vorticity persist as remnants of the low speed boundary layer. The collective interaction of these small scale vortices, merging into larger scale structures, largely controls the dynamics of the shear layer. Further computational details are given in Ref. 15.

CONCLUDING REMARKS

The CFD validation activity at NASA Lewis is a balanced effort between the conduct of experimental research and the development of computational tools. The program has been briefly described by high-lighting research efforts in three areas; namely: Inlets, Ducts and Nozzles; Turbomachinery; and Chemically Reacting Flows. Much of the computational focus for the Inlets, Ducts and Nozzles has been on the development and validation of parabolized Navier-Stokes codes. In the future, more emphasis will be placed on three-dimensional Reynolds averaged Navier-Stokes methods. The experimental effort will continue to provide a fundamental understanding of the fluid flow physics,

to develop new and/or improved flow models, and to provide benchmark datasets for validation of both parabolized and Reynolds averaged Navier-Stokes methods.

In the turbomachinery area, the program encompasses a variety of computational and experimental approaches. Special emphasis is placed on the Reynolds averaged Navier-Stokes equations, the unsteady Euler equations and the average passage equations. The experimental emphasis is on high response time-resolved measurements and on measurements within rotating machinery blade passages.

Activity in chemical reacting flow research is focused on fluid mechanics, combustion chemistry and turbulence/combustion interaction. Emphasis is placed on Reynolds averaged Navier-Stokes solvers and Direct Numerical simulation. The experimental activity includes unsteady reacting flows, shock tube kinetics and multiphase flow phenomena.

In conclusion, it is noted that as numerical methods are improved and the ability to compute complex fluid physics is enhanced, it is critical that the users be aware of the code validity and limitations. These limitations can only be established by a careful, systematic evaluation of each numerical scheme. A coupled series of experiments must be conducted in close collaboration with the numerical approach in order to assess if the code can predict the critical physics. The exact nature of the measured surface and flow field quantities required is highly dependent on the problem under investigation, i.e., aerodynamics, heat transfer or reacting flows. The experiments in this paper are the type required for the CFD assessment and validation process.

REFERENCES

1. Bradley, R.G., et al: "Computational Fluid Dynamics Validation. Report prepared for NASA's Aeronautics Advisory Committee, Mar. 22, 1987.

2. Povinelli, L.A.: Assessment of Three-Dimensional Inviscid Codes and Loss Calculations for Turbine Aerodynamic Computations. Gas Turbines Power, vol. 107, no. 2, Apr. 1985, pp. 265-276. (NASA TM-83571).

3. Povinelli, L.A.: "Validation of Viscous and Inviscid Computational Methods for Turbomachinery Components. ASME Paper 86-GT-42, June 1986. (NASA TM-87193).

4. Povinelli, L.A.; and Towne, C.E.: Viscous Analyses for Flow Through Subsonic and Supersonic Intakes. Engine Response to Distorted Inflow Conditions, AGARD CP-400, AGARD, Nevilly-Sur-Seine, France, 1986, pp. 5-1 to 5-20. (NASA TM-88831).

5. Povinelli, L.A.; and Anderson, B.H.: Investigation of Mixing in a Turbofan Exhaust Duct, Part II: Computer Code Application and Verification. AIAA J., vol. 22, no. 4, Apr. 1984, pp. 518-525.

6. Abbott, J.M.; Anderson, B.H.; and Rice, E.J.: Inlets, Ducts and Nozzles. Aeropropulsion '87, NASA CP-10003, 1987.

7. Chriss, R.M., et al.: An LDA Investigation of Three-Dimensional Normal Shock-Boundary Layer Interactions in a Corner. AIAA Paper 87-1369, June 1987.

8. Kunik, W.G.: Application of a Computational Model for Vortex Generators in Subsonic Internal Flows. AIAA Paper 86-1458, June 1986. (NASA TM-87327).

9. Simoneau, R.J., et al: Turbomachinery. Aeropropulsion '87, NASA CP-10003, 1987.

10. Chima, R.V.: Explicit Multigrid Algorithm for Quasi-Three-Dimensional Viscous Flows in Turbomachinery. J. Propulsion Power, vol. 3, no. 5, Sept.-Oct. 1987, pp. 397-405.

11. Wood, J.R.; Strazisar, A.J.; and Simonyi, P.S.: Shock Structure Measured in a Transonic Fan Using Laser Anemometry. Transonic and Supersonic Phenomena in Turbomachines, AGARD CP-401, AGARD, Nevilly Sur-Seine, France, 1986.

12. Hathaway, M.D., et al.: Rotor Wake Characteristics of a Transonic Axial-Flow Fan. AIAA J., vol. 24, no. 11, Nov. 1986, pp. 1802-1810.

13. Mularz, E.J.; and Sockol, P.M.: Chemical Reacting Flows. Aeropropulsion '87, NASA CP-10003, 1987.

14. Bulzan, D.L.; Shuen, J.S.; and Faeth, G.M.: Particle-Laden Swirling Free Jets: Measurement and Prediction. AIAA Paper 87-0303, Jan. 1987. (NASA TM-88904).

15. Claus, R.W.; Huang, P.G.; and MacInnes, J.: "Time-Accurate Simulations of a Mixing Layer Forced at a Single Frequency. AIAA Paper 88-061, Jan. 1988.

TABLE I. - INLET, DUCT AND NOZZLE CFD VALIDATION

Code and critical models requiring validation		Experimental program elements
CFD codes by class	Critical flow physics models	
Three-dimensional subsonic PNS	Turbulence Separation Vortex generation	Transition ducts Offset ducts Vortex generators
Three-dimensional subsonic/ hypersonic PNS	Turbulence Separation Real gas effects Boundary layer bleed Boundary layer transition	Shock-boundary layer interaction Boundary-layer bleed High temperature flow
Three-dimensional Navier-Stokes	Turbulence Real gas effects Boundary layer transition	Above experiments Separation flow physics Enhanced jet mixing

TABLE II. - TURBOMACHINERY CFD VALIDATION

Code and critical models requiring validation		Experimental program elements
CFD code by class	Flow physics models	
Steady Euler	End-wall boundary layer Blade surface boundary layer Shock boundary layer interaction	High-speed turbomachinery Low-speed turbomachinery Two-dimensional cascade Shock boundary layer interaction
Steady Navier-Stokes	Turbulence Boundary layer transition	Two-dimensional cascade Low-speed centrifugal Low-speed boundary layer Three-dimensional heat transfer Low-speed axial turbomachinery
Passage-average Navier-Stokes	Turbulence Other closure models	Low-speed multistage High-speed multistage
Unsteady Navier-Stokes (rotor/stator)	Turbulence Boundary layer transition	Low-speed turbomachinery High-speed turbomachinery

TABLE III. - CHEMICALLY REACTING FLOWS CFD VALIDATION

Code and critical models requiring validation		Experimental program element
CFD codes by class	Critical flow physics models	
Steady Navier-Stokes	Fuel spray Turbulence Turbulence/combustion Chemical kinetics interaction Radiation/soot formation	Multiphase flow research: phase interaction
Time accurate Navier-Stokes	Turbulence Turbulence/combustion interaction Chemical kinetics	Planar reacting shear layer: Turbulence/combustion interaction Soot/radiation characteristics
Direct numerical Simulation	Chemical kinetics	Shock tube chemical kinetics

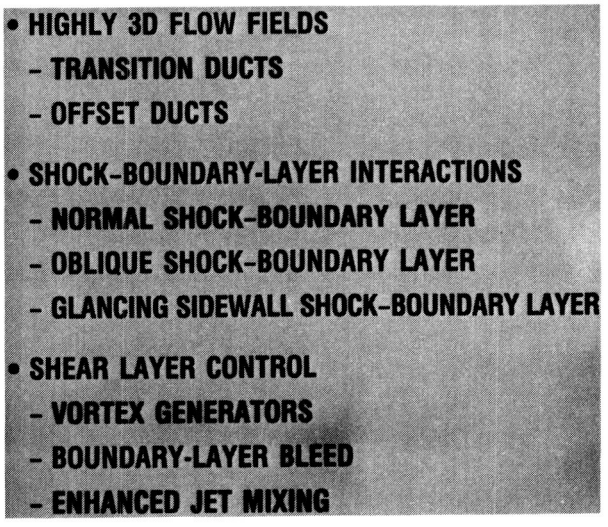

FIGURE 1. - INLETS, DUCTS, AND NOZZLES. FLOW PHENOMENA.

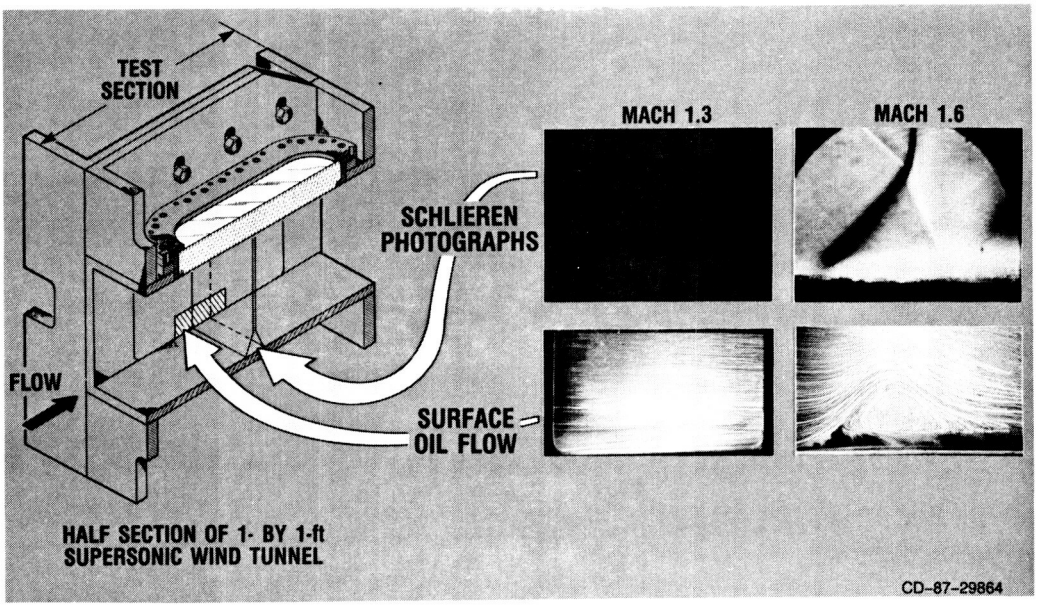

FIGURE 2. - NORMAL SHOCK-BOUNDARY-LAYER INTERACTION.

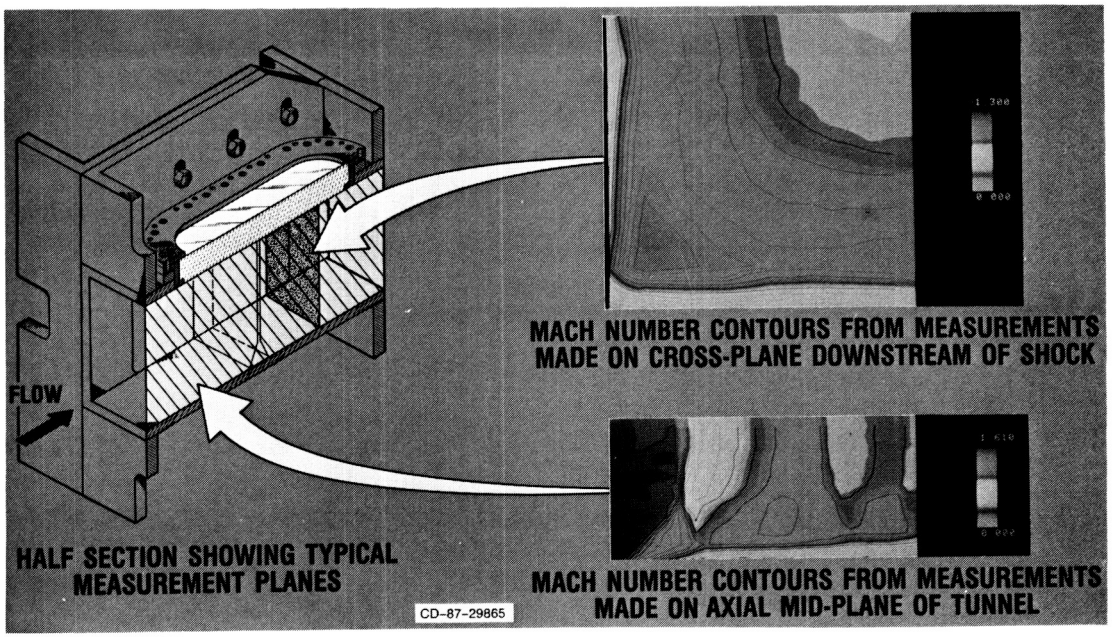

FIGURE 3. - RESULTS OF LASER ANEMOMETER MEASUREMENTS FOR NORMAL SHOCK-BOUNDARY LAYER INTERACTION AT MACH NUMBER 1.6.

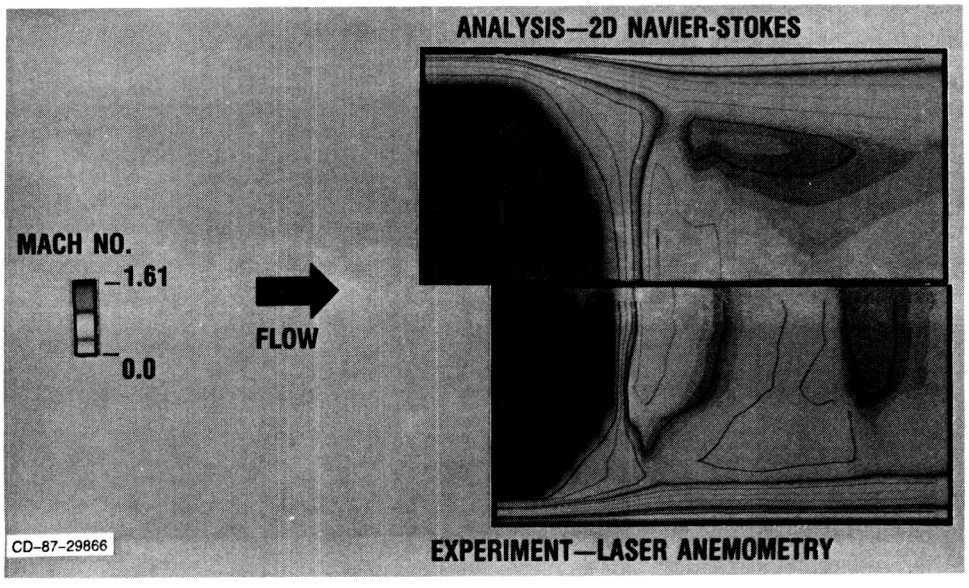

FIGURE 4. - MACH 1.6 NORMAL SHOCK WAVE BOUNDARY LAYER INTERACTION. COMPARISON OF LDV EXPERIMENT AND ANALYSIS.

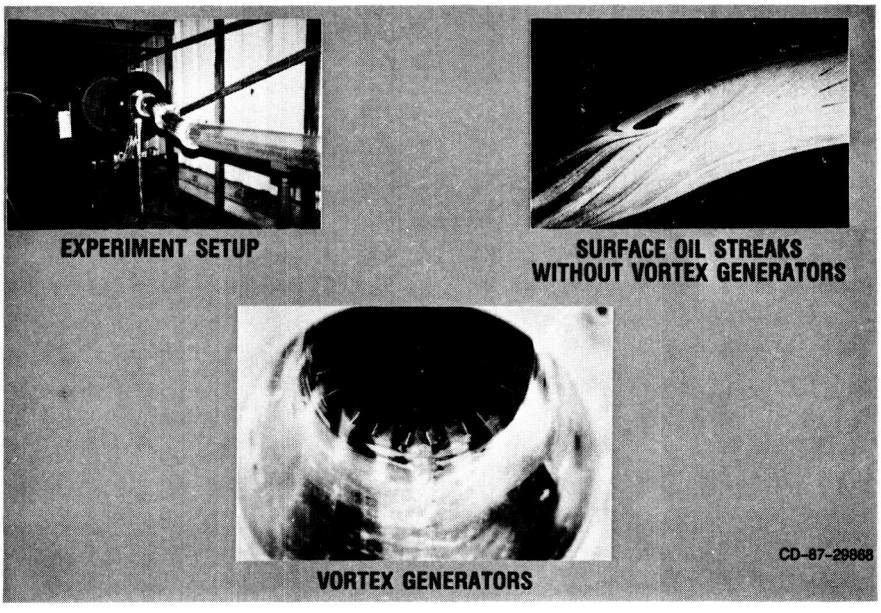

FIGURE 5. - VORTEX GENERATORS IN DIFFUSING OFFSET DUCT. L/D = 5.0; OFFSET/D = 1.34; A_{EXIT}/A_{INLET} = 1.50.

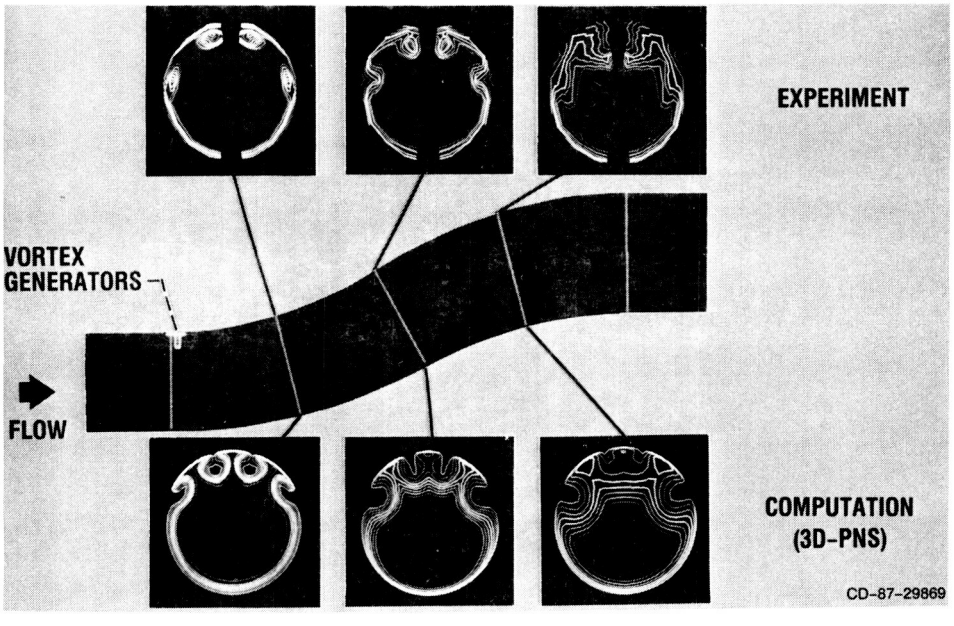

FIGURE 6. - VORTEX GENERATORS IN DIFFUSING OFFSET DUCT - COMPARISON OF ANALYSIS AND EXPERIMENT. TOTAL PRESSURE CONTOURS: M = 0.6.

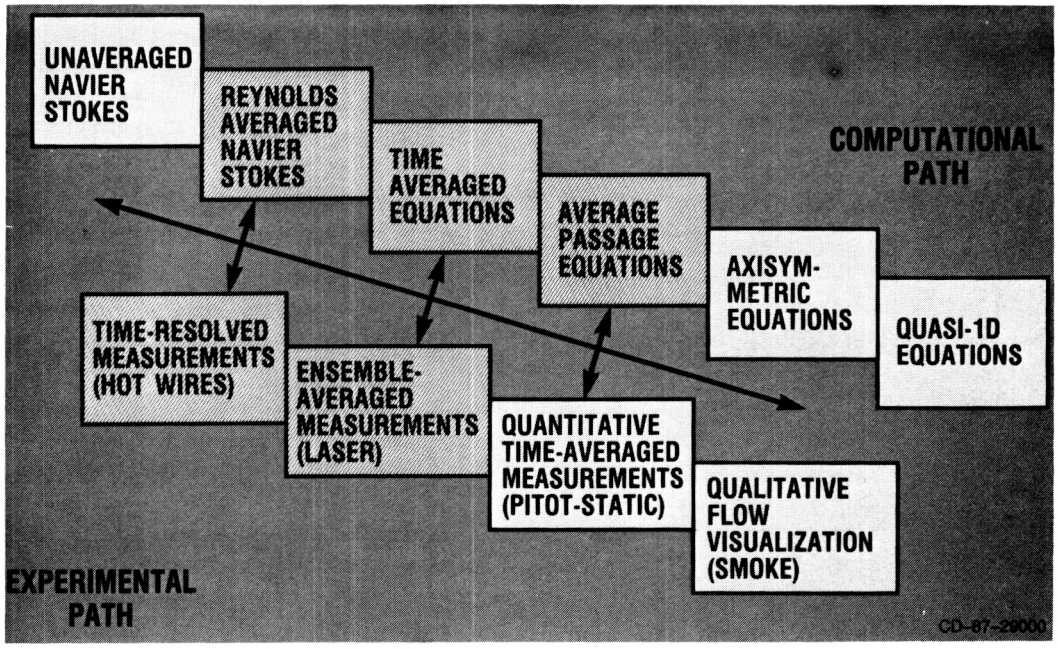

FIGURE 7. - POSITION OF THE TURBOMACHINERY PROGRAM ON COMPUTATIONAL AND EXPERIMENTAL PATHS.

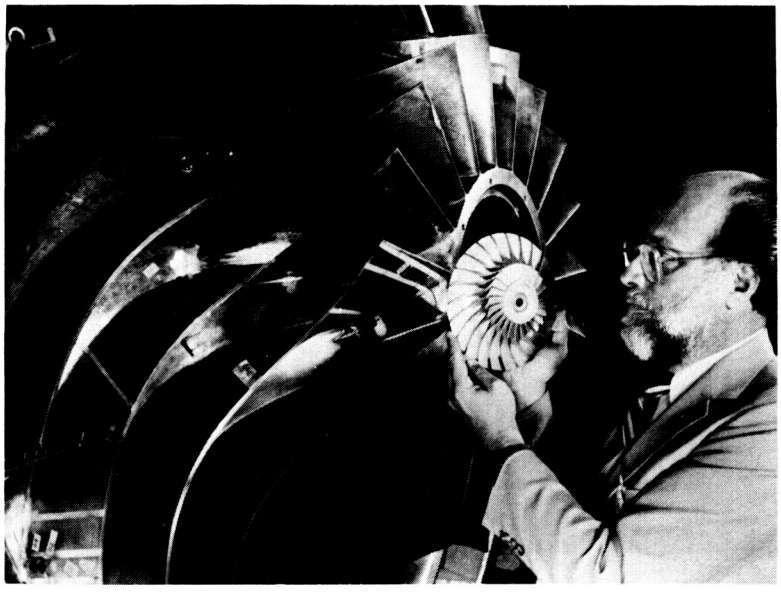

FIGURE 8. - LARGE LOW-SPEED CENTRIFUGAL COMPRESSOR NEW FLOW PHYSICS AND CODE VALIDATION RIG.

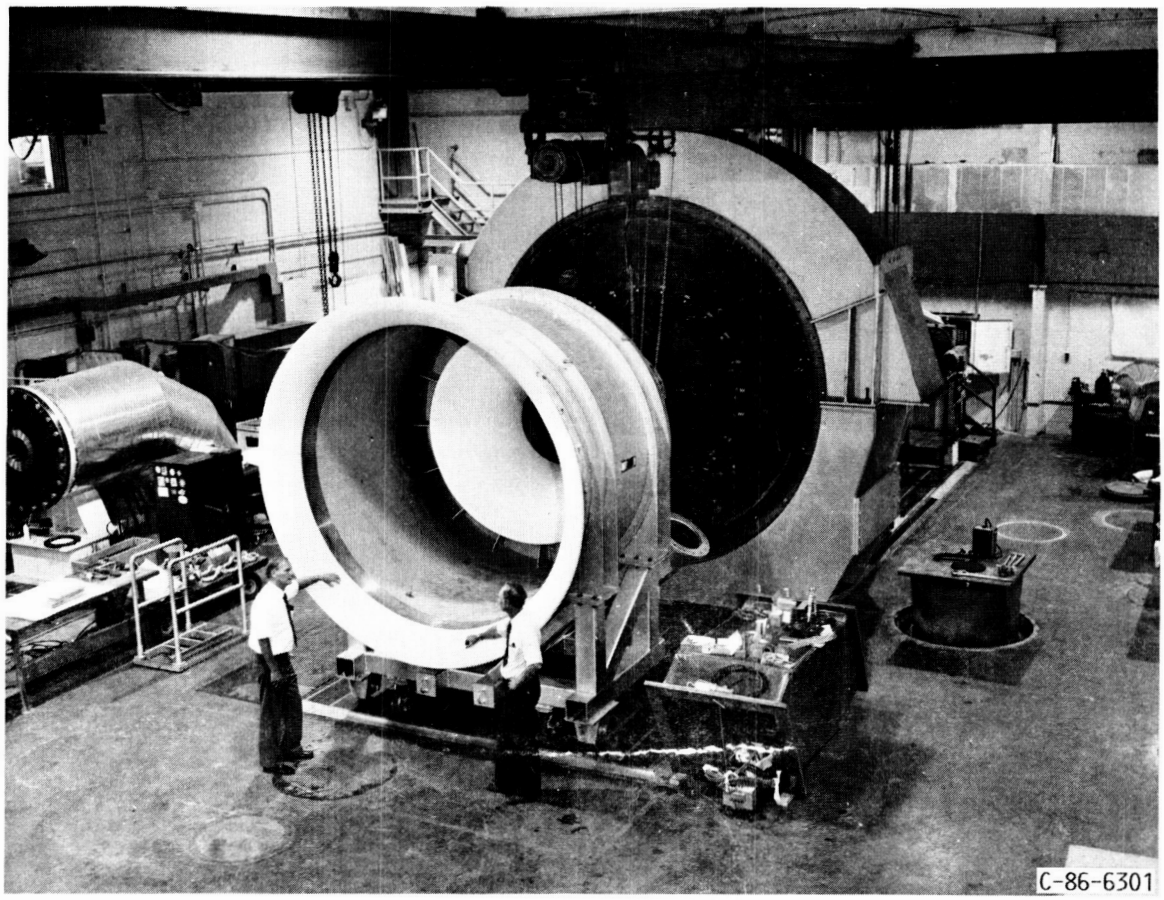

FIGURE 9. - LARGE LOW SPEED CENTRIFUGAL COMPRESSOR APPARATUS. PLENUM AND BELLMOUTH.

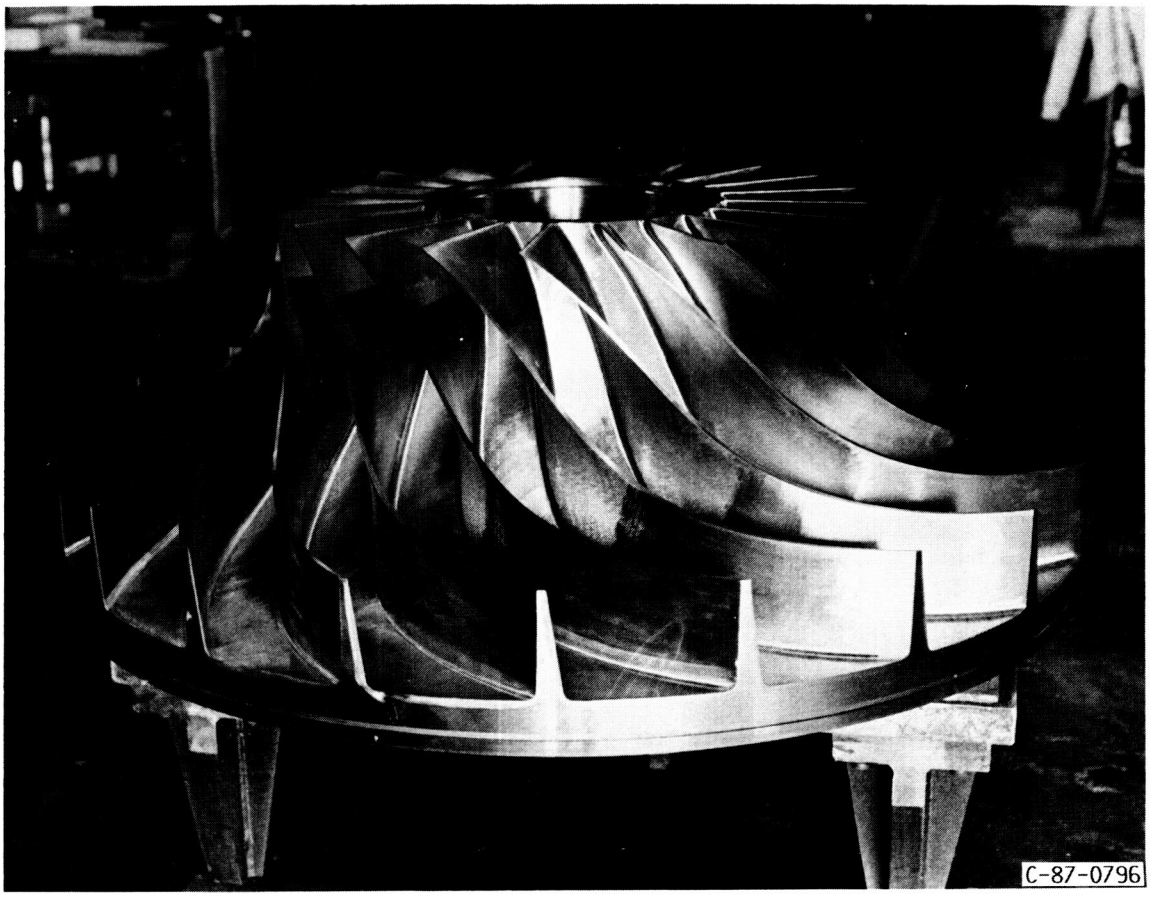

FIGURE 10. - LARGE LOW SPEED CENTRIFUGAL COMPRESSOR ROTOR.

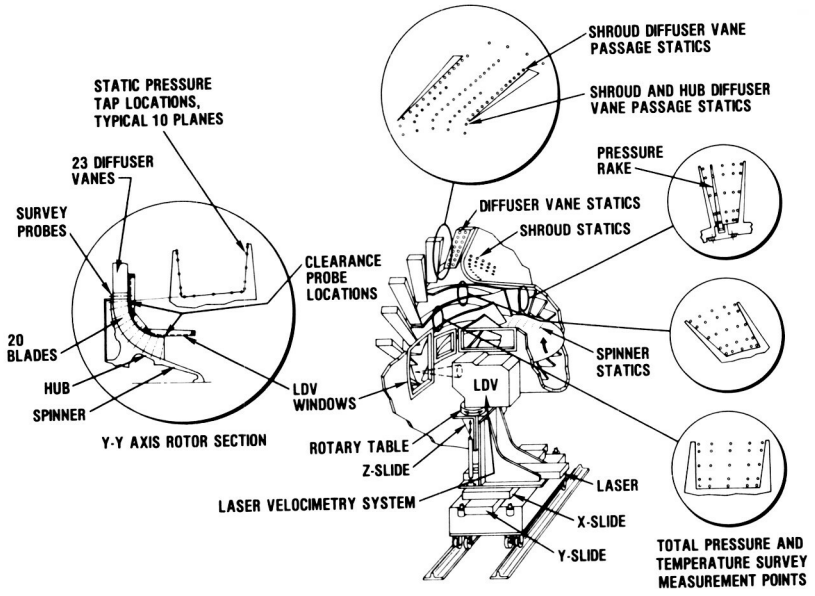

FIGURE 11. - LOW-SPEED CENTRIFUGAL COMPRESSOR INSTRUMENTATION.

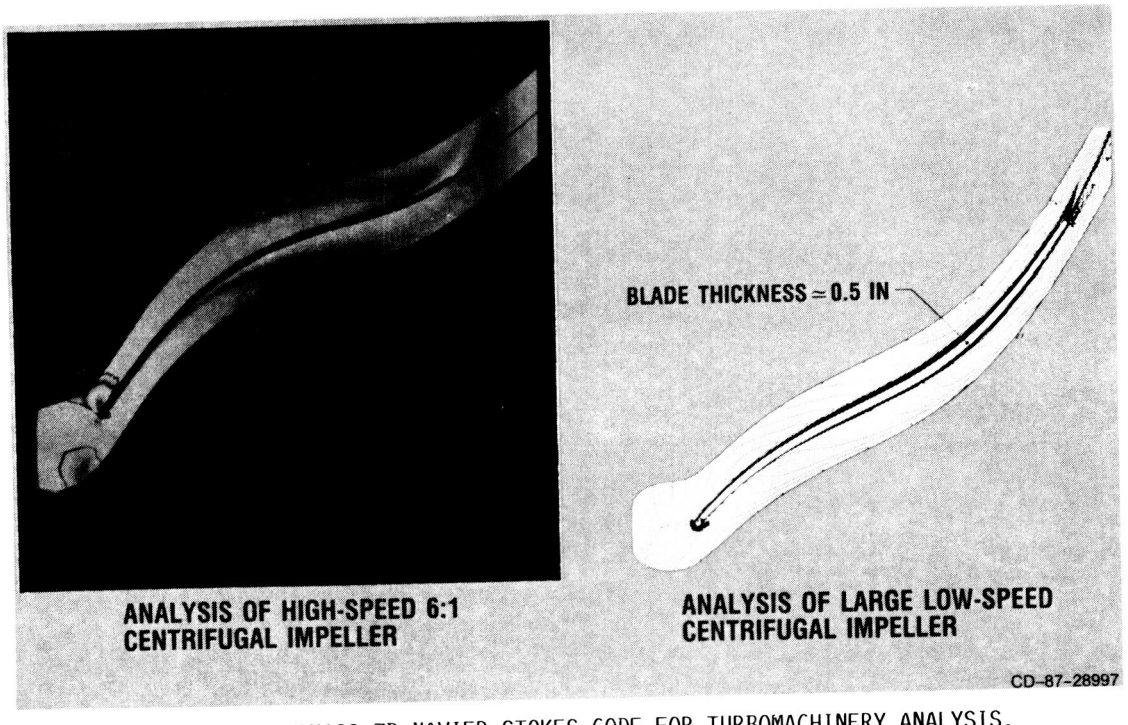

FIGURE 12. - QUASI-3D NAVIER-STOKES CODE FOR TURBOMACHINERY ANALYSIS.

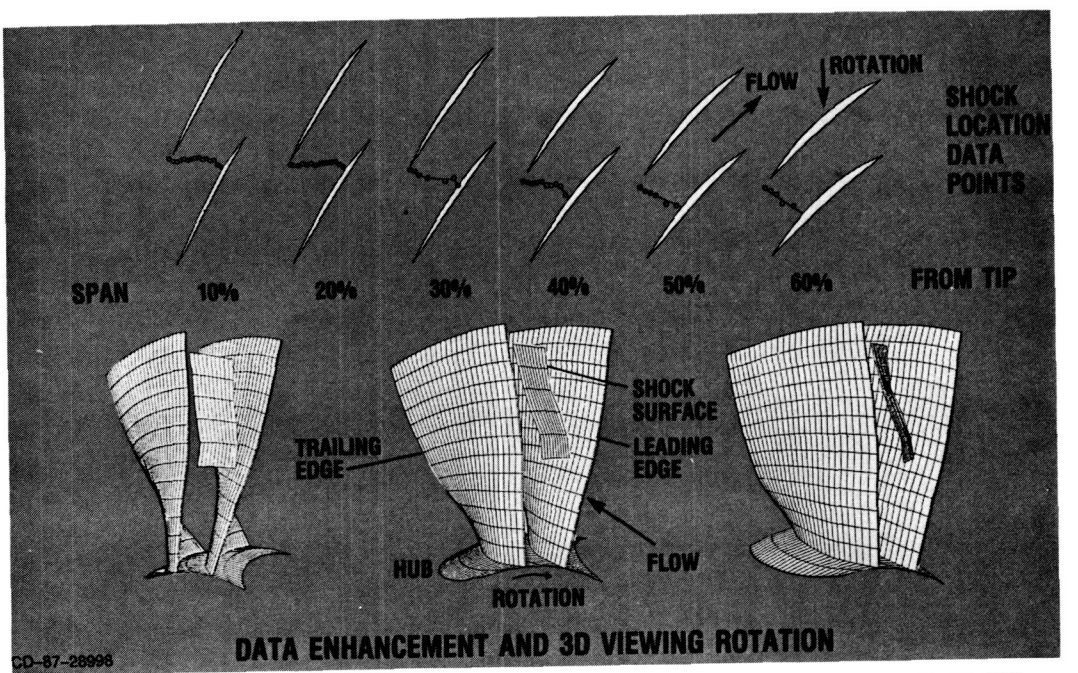

FIGURE 13. - MEASUREMENT OF 3D SHOCK STRUCTURE IN A TRANSONIC AXIAL-FLOW FAN.

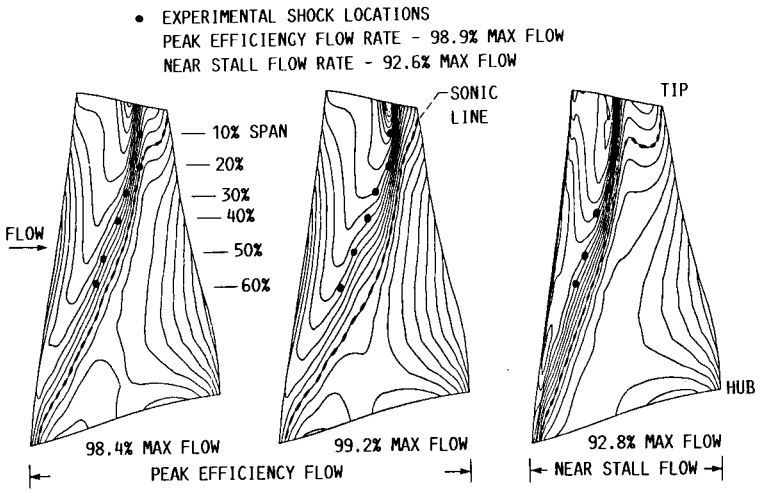

(A) COMPARISON OF SHOCK LOCATIONS ON THE BLADE SUCTION SURFACE FOR PEAK EFFICIENCY AND NEAR STALL FLOW RATES WITH ISOMACH LINES FROM A 3D EULER CALCULATION.

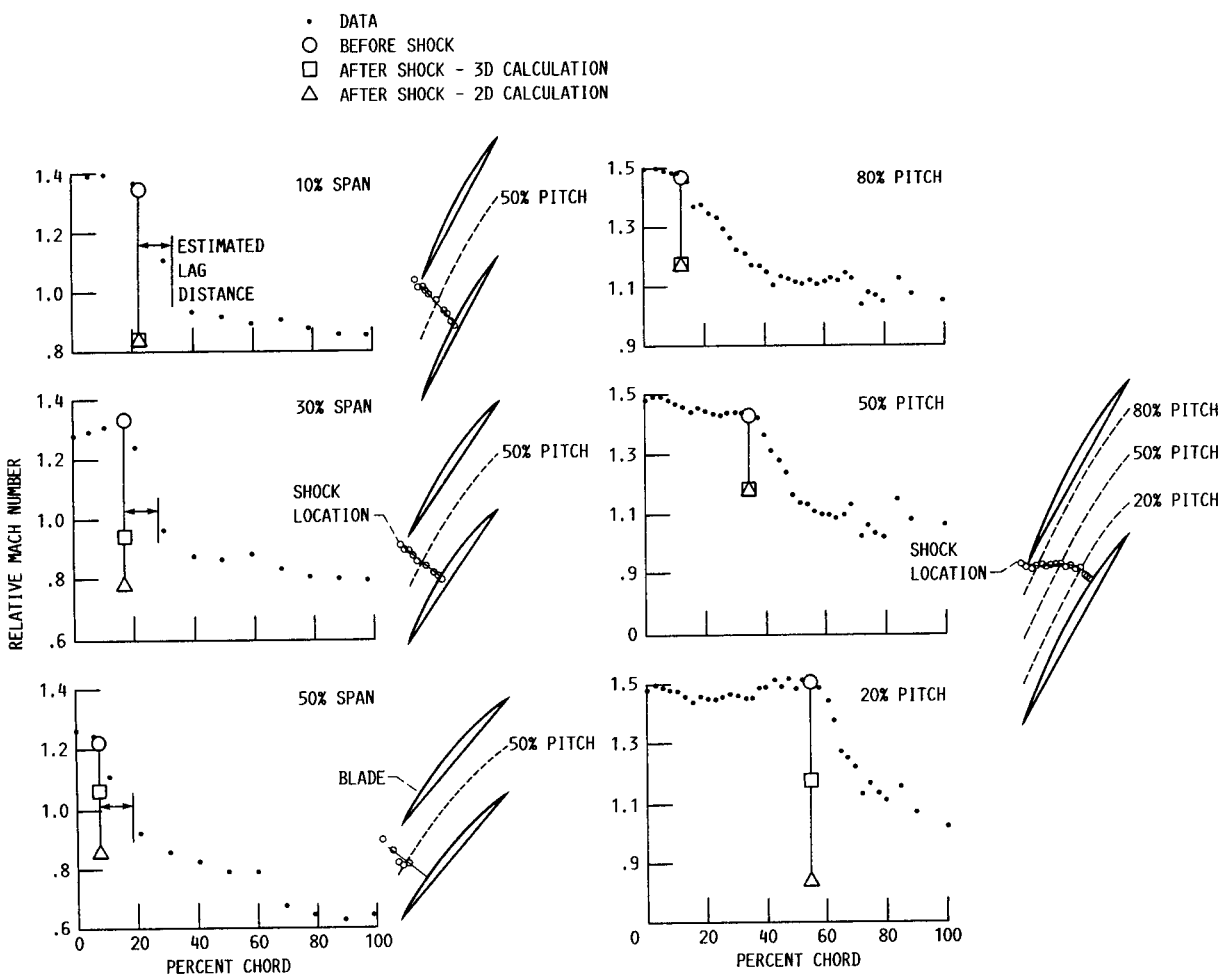

(B) CHORDWISE PLOTS OF RELATIVE MACH NUMBER AT 50% PITCH FOR THE NEAR STALL FLOW RATE AT 10%, 30%, AND 50% SPAN.

(C) CHORDWISE PLOTS OF RELATIVE MACH NUMBER AT 10% SPAN FOR THE PEAK EFFICIENCY FLOW RATE AT 20%, 50%, AND 80% PITCH FROM THE SUCTION SURFACE.

FIGURE 14. - COMPARISON OF COMPUTATIONAL AND EXPERIMENTAL RESULTS FOR A TRANSONIC ROTOR.

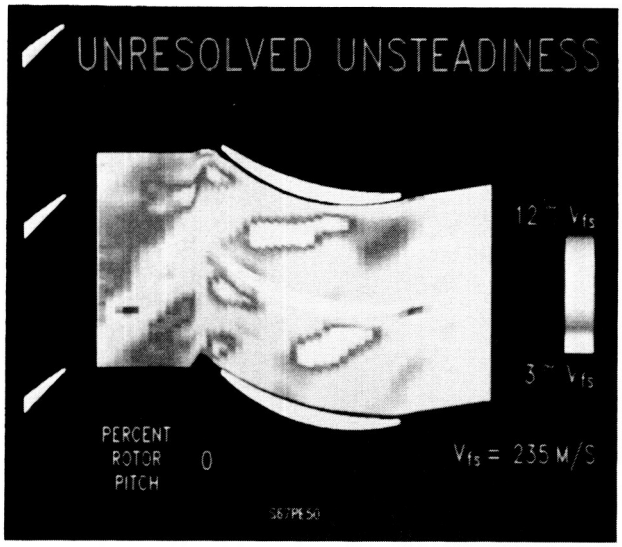

FIGURE 15. - COMPRESSOR "TURBULENT" KINETIC ENERGY DISTRIBUTION. ONE FRAME FROM DATA MOVIE SHOWING THE PROGRESS OF A WAKE THROUGH A STATOR PASSAGE DOWNSTREAM OF THE ROTOR.

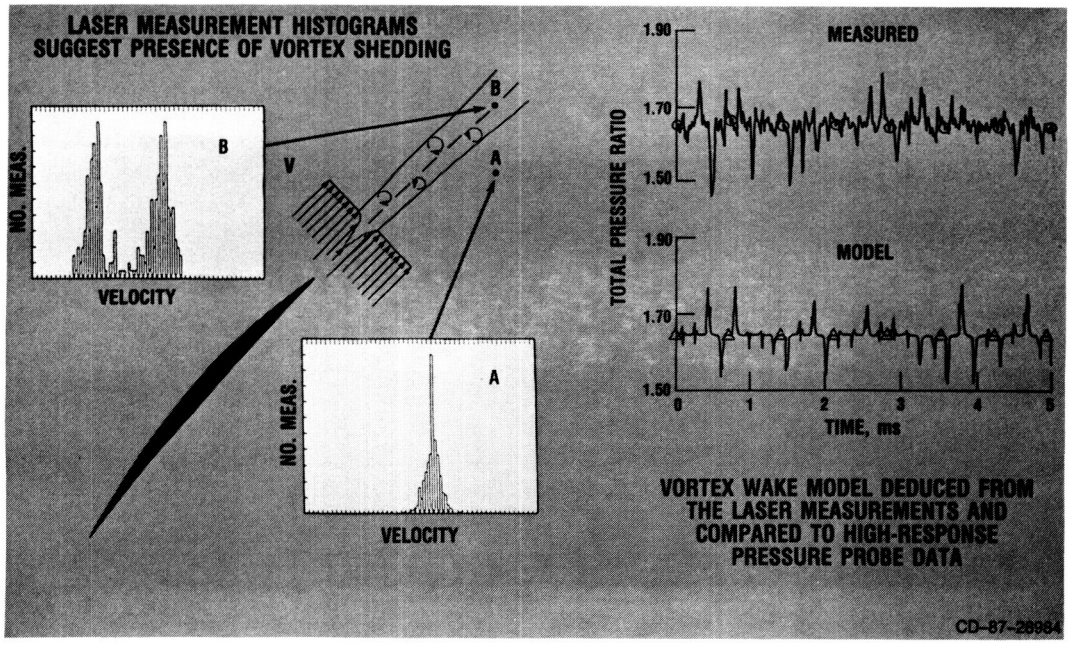

FIGURE 16. - FAN ROTOR VORTEX SHEDDING DEVELOPING MODELS TO EXPLAIN FLOW PHYSICS.

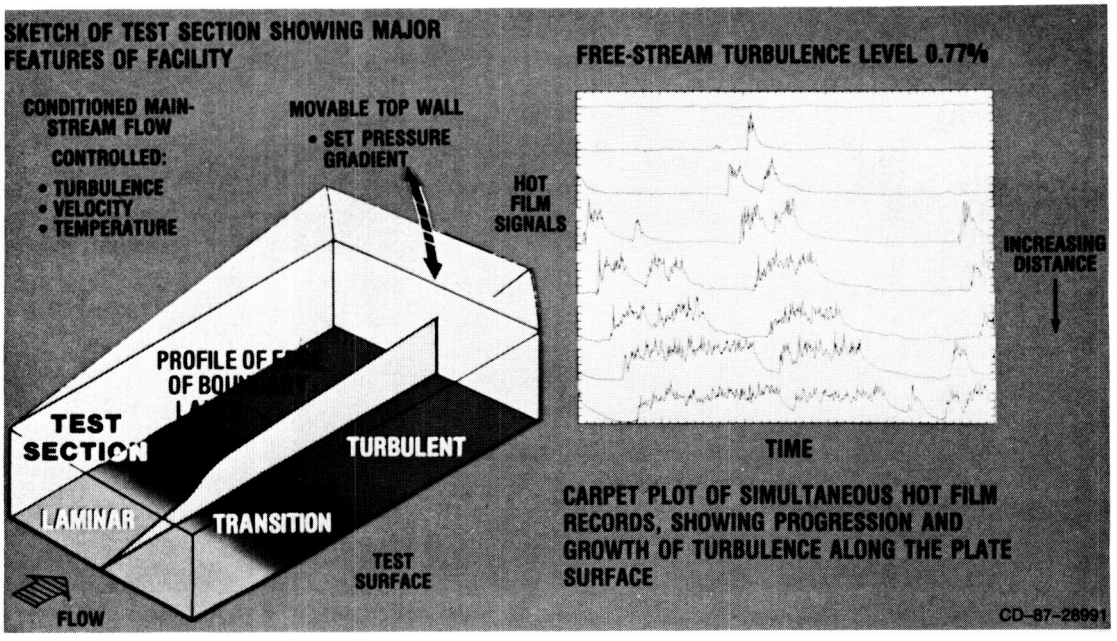

FIGURE 17. - BOUNDARY-LAYER TRANSITION RESEARCH - A STUDY OF INTERMITTENT BEHAVIOR.

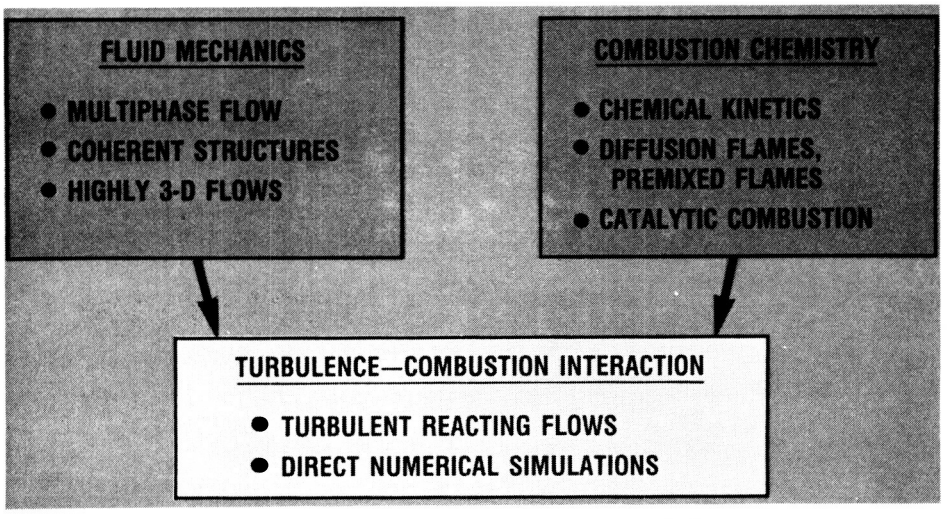

FIGURE 18. - CHEMICAL REACTING FLOWS.

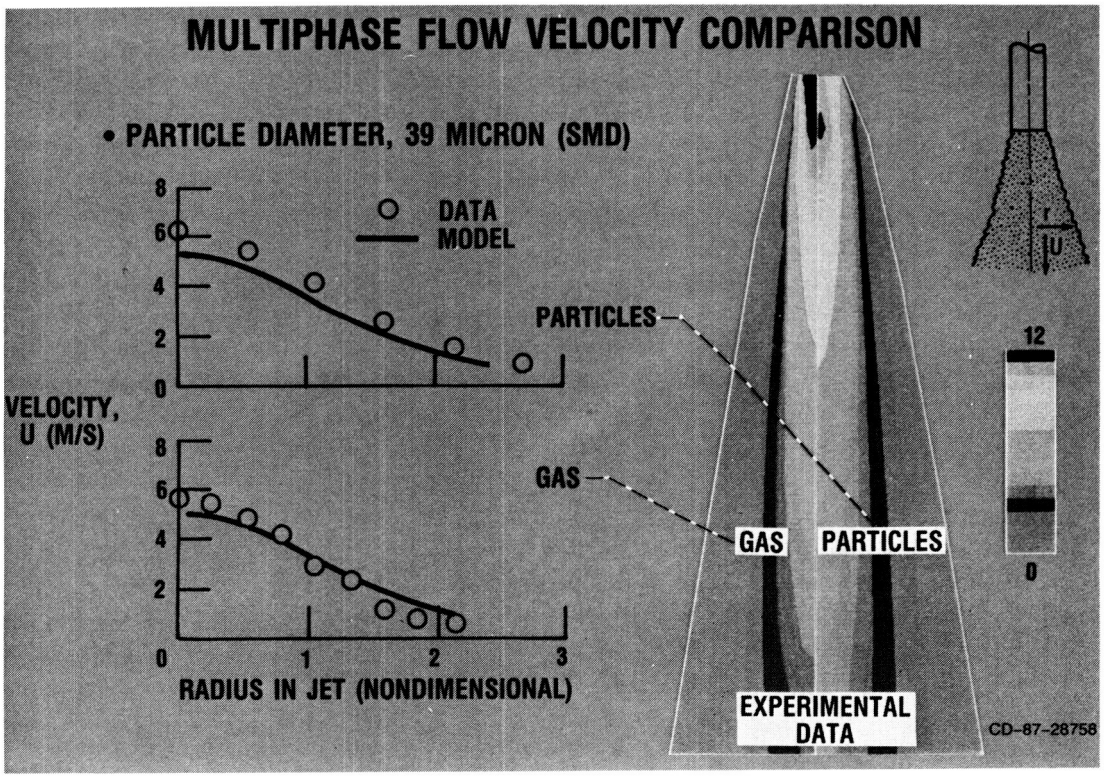

FIGURE 19. - MULTIPHASE FLOW VELOCITY COMPARISON.

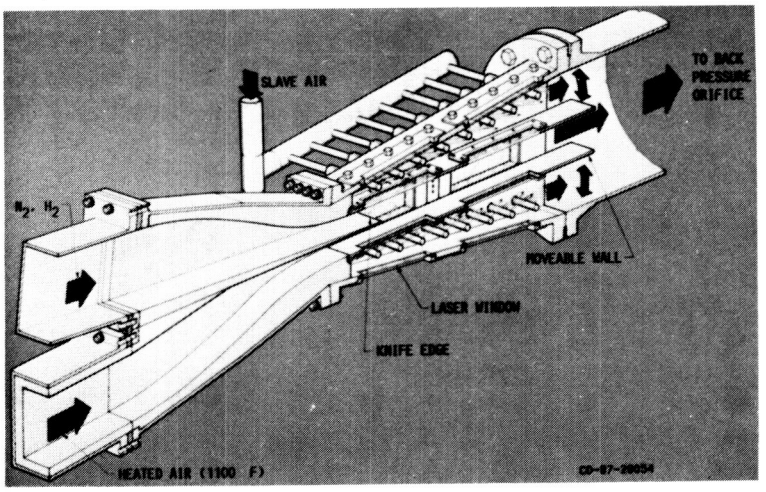

FIGURE 20. - PLANAR REACTING SHEAR LAYER TEST SECTION.

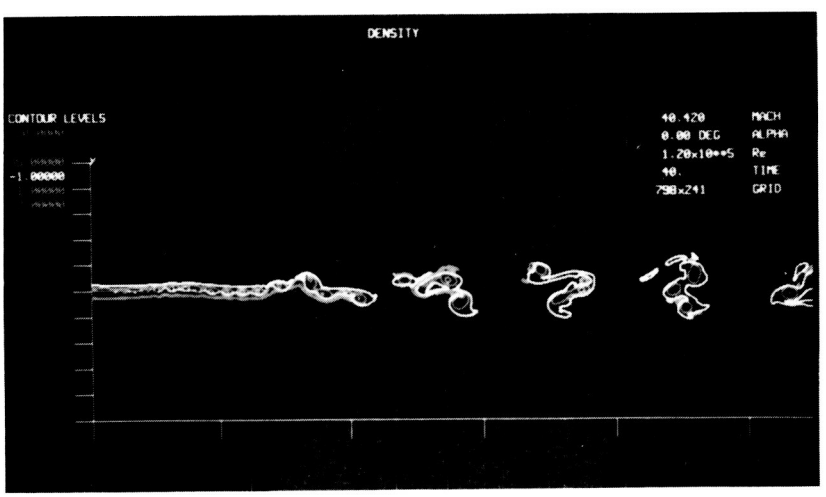

FIGURE 21. - COMPUTER CODE RESULTS OF TWO STREAM FREE SHEAR LAYER SHOWING VORTICITY STRUCTURE.

NASA
National Aeronautics and Space Administration

Report Documentation Page

1. Report No.	2. Government Accession No.	3. Recipient's Catalog No.
NASA TM-100797		

4. Title and Subtitle	5. Report Date
CFD Validation Experiments for Internal Flows	6. Performing Organization Code

7. Author(s)	8. Performing Organization Report No.
Louis A. Povinelli	E-3973
	10. Work Unit No. 505-62-21

9. Performing Organization Name and Address	11. Contract or Grant No.
National Aeronautics and Space Administration Lewis Research Center Cleveland, Ohio 44135-3191	13. Type of Report and Period Covered Technical Memorandum

12. Sponsoring Agency Name and Address	14. Sponsoring Agency Code
National Aeronautics and Space Administration Washington, D.C. 20546-0001	

15. Supplementary Notes

Prepared for the Symposium on Validation of Computational Fluid Dynamics sponsored by the AGARD Fluid Dynamics Panel, Lisbon, Portugal, May 2-5, 1988.

16. Abstract

CFD validation experiments at NASA Lewis Research Center are described in this paper. The material presented summarizes the research in three areas: Inlets, Ducts and Nozzles; Turbomachinery; and Chemically Reacting Flows. The specific validation activities are concerned with shock-boundary layer interactions, vortex generator effects, large low speed centrifugal compressor measurements, transonic fan shock structure, rotor/stator kinetic energy distributions, stator wake shedding characteristics, boundary layer transition, multiphase flow and reacting shear layers. These experiments are intended to provide CFD validation data for the internal flow fields within aerospace propulsion system components.

17. Key Words (Suggested by Author(s))	18. Distribution Statement
CFD validation Internal fluid mechanics Propulsion CFD	Unclassified - Unlimited Subject Category 02

19. Security Classif. (of this report)	20. Security Classif. (of this page)	21. No of pages	22. Price*
Unclassified	Unclassified	22	A02

*For sale by the National Technical Information Service, Springfield, Virginia 22161